Journal of Applied Research and Technology

www.jart.icat.unam.mx

Journal of Applied Research and Technology 21 (2023) 447-456

Original

Properties of hydroxyapatite from tilapia (*Oreochromis niloticus*) bones: An approach towards its potential use as a dye adsorbent

B. G. González-González[a] • C. O. García-Sifuentes[b*] • H. Santacruz-Ortega[a] • F. Brown-Bojórquez[a] • R. E. Navarro-Gautrín[a] • R. Sugich-Miranda[c] • E. Carvajal-Millán[d]

[a]*Department of Polymers and Materials Research, University of Sonora (UNISON), Hermosillo, Sonora, Mexico*
[b]*Fishery Products Quality Laboratory, Research Center for Food and Development, A.C. (CIAD), Hermosillo, Sonora, México*
[c]*Department of Chemical-Biological Sciences, University of Sonora (UNISON), Hermosillo, Sonora, México*
[d]*Biopolymers, Research Center for Food and Development (CIAD), Hermosillo, Sonora, Mexico*

Received 01 18 2022; accepted 06 07 2022
Available 06 30 2023

Abstract: The properties of hydroxyapatite (HAp) obtained from tilapia (*Oreochromis niloticus*) bones and its potential use as a dye adsorbent using methyl orange (MO) as a model dye were evaluated. HAp was produced by the calcination of dried tilapia bones at 900 °C for 4 h. Then, HAp was characterized using thermogravimetric (TGA) and differential thermogravimetric (dTG) analyses, Fourier transform infrared spectroscopy (FTIR), field emission scanning electron microscopy (FESEM) and energy dispersive spectroscopy (EDS), transmission electron microscopy (TEM), x-ray diffraction (XRD), among others. The HAp obtained was used for MO dye adsorption in a batch process. The yield of HAp was 51.6%. FTIR showed characteristic bands of functional groups of HAp [OH^- and $(PO_4)^{3-}$]. FESEM images showed HAp with different morphologies and a porous surface. The EDS analysis indicated the presence of calcium and phosphorus with an atomic ratio of Ca/P of 1.60, TEM images revealed the formation of agglomerates and an average particle size of 655.1 nm. HAp and β-tricalcium phosphate (β-TCP) phases were identified through XRD. The HAp point of zero charge (pH_{pzc}) was 9.7 indicating a possible adsorption of anionic dyes at pH< pH_{pzc} and cationic dyes at pH> pH_{pzc}. The HAp was able to successfully adsorb 82.6% of MO dye from aqueous solution. These findings demonstrated that the HAp obtained from tilapia *(Oreochromis niloticus)* bones possesses suitable properties to be used as a potential material to remove dyes.

Keywords: Hydroxyapatite, calcination, dye adsorbent, tilapia, fishery by-product

*Corresponding author.
E-mail address: sifuentes@ciad.mx (C.O García-Sifuentes).
Peer Review under the responsibility of Universidad Nacional Autónoma de México.

1. Introduction

Synthetic dyes are widely used in various industries, mainly the textile industry. Annually 70 million tons of dyes are produced worldwide (Benkhaya et al., 2020). About 10% of dyestuff is discharged to the environment from textile industry effluents after dyeing processes. Methyl orange (MO) is a toxic anionic dye widely used in the textile industry, its acute exposure can cause vomiting, shock, cyanosis, jaundice, quadriplegia, and tissue necrosis in humans (Darwish et al., 2019). Therefore, removing MO dyes before being poured into water bodies is crucial (Aljeboree et al., 2017; Benkhaya et al., 2020).

Several dye removing methods include physical, chemical, and biological processes such as adsorption (Adeogun et al., 2018), coagulation-flocculation (Dotto et al., 2019), oxidation (Tony, 2020), biological degradation (Ceretta et al., 2020), and others. The adsorption approach stands out due to its effectiveness, ease of operation, low-cost and reusable absorbents (Aljeboree et al., 2017). Hence, it could be considered a convenient technology to treat wastewater discarded by the textile industry.

Recently, the fabrication of new adsorbent materials from natural sources has gained interest (Akhouairi et al., 2019; Chaari et al., 2019), especially for those made from industrial by-products due to their abundance, low cost, good mechanical, and chemical resistance (Bensalah et al., 2020). In this sense, natural hydroxyapatite [$Ca_{10}(PO_4)_6(OH)_2$, HAp)] studied for biomedical applications (Da Cruz et al., 2020; Paul, Pal, Choudhury, Balla, et al., 2017; Paul, Pal, Choudhury, Bodhak, et al., 2017) is also attracting attention as a potential dye adsorbent (Bee & Hamid, 2020; Dotto et al., 2019). It has the ability of ionic exchange and exhibits affinity of adsorption towards diverse pollutants (Bee & Hamid, 2020); for instance, ionic dyes can be removed by calcium (positive charge) and phosphate ions (negative charge) contained in HAp.

Different studies to obtain hydroxyapatite from by-products and remove dyes from aqueous solutions have been performed. For example, Bensalah et al. (2020) synthesized HAp from industrial waste phosphogypsum to remove Congo red dye; Adeogun et al. (2018) applied HAp from eggshell as an adsorbent for reactive yellow 4; El Haddad et al. (2012) calcinated animal bones and produced HAp to adsorb basic red 12. However, few studies on the synthesis of HAp from fishery by-products such as bones and scales have been conducted for dye adsorption (Peng et al., 2017; Swamiappan et al., 2021; Uzunoğlu & Özer, 2016).

Tilapia is the second-largest farmed finfish in the world after carp. Within this group, *Oreochromis niloticus* is the most important species in global aquaculture with a production of 4,525,400 metric tons in 2018, representing 8.3% of total farmed fish production (Abdel-Ghany et al., 2019; FAO, 2020). Consequently, the bones from tilapia (*Oreochromis niloticus*) can reach 678,810 tons, that is, 15% of total fish weight (FAO, 2020). Therefore, these bones could be an alternative to raw material for the development of new adsorbent materials and contribute to the reduction of the environmental impact generated by fishery industrial waste. This study aims to analyze the properties of HAp obtained from tilapia (*Oreochromis niloticus*) bones for its potential use as a dye adsorbent using methyl orange (MO) as a model.

2. Materials and methods

2.1. Obtention of hydroxyapatite (HAp)

Tilapia (*Oreochromis niloticus*) skeletons were processed in a deboning machine to remove most of the meat adhered to bones and the remaining meat and fat were removed by boiling water. After that, bones were filtered, dried, blended and sieved (≤ 150 µm particle size). Tilapia bones were calcinated at 900 °C for 4 h using an electric muffle furnace (Thermolyne F6000) to obtain HAp. After that, the calcinated sample was cooled in the furnace; the HAp yield was calculated taking the weight before and after calcination as a basis.

2.2. Identification and characterization of HAp

2.2.1. Thermogravimetric (TGA) and differential thermogravimetric (dTG) analyses

The thermal decomposition process of tilapia bones to obtain HAp was monitored through sample weight loss. The assay was performed by a thermogravimetric analyzer (Perkin Elmer, Pyris 1) using a temperature range from 20 to 850 °C with a heating rate of 10 °C/min under an air atmosphere.

2.2.2. Fourier transform infrared spectroscopy (FTIR)

HAp functional groups were monitored with FTIR. For that, the KBr pellet method was applied using an FTIR spectrophotometer (Perkin Elmer Frontier™). The spectra were obtained in the wavenumber range of 4000–400 cm^{-1} and analyzed with Spectrum™ 10 software.

2.2.3. Field emission scanning electron microscopy (FESEM)

HAp surface morphology was analyzed with micrographs obtained with a JEOL JSM-78 00F field emission scanning electron microscope (FESEM). The elemental composition of HAp was analyzed through a scanning electron microscope (JOEL JSM-5410LV, with a 20 kV operating voltage) coupled with energy dispersive microscopy (EDS) using an Oxford X-Max detector. The atomic Ca/P of HAp was confirmed by X-ray photoelectron spectroscopy (XPS) using an X-ray photoelectron spectrometer (Perkin Elmer, Physical Electronics PHI 5100) with a non-monochromatic MgKα X-ray source (1256 eV).

2.2.4. Transmission electron microscopy (TEM)

Crystal morphology was assessed using a transmission electron microscope (JEOL JEM 2010F, accelerating voltage of 200 kV). The particle size was estimated from TEM images with the software ImageJ.

2.2.5. X-ray diffraction (XRD)

X-ray diffraction was used to identify the crystalline structure and phase composition of HAp. Patterns were obtained using a diffractometer (BRUKER AXS D8 Advance) equipped with CuKα as a radiation source. Data were collected in a range of 10-70° (2θ); with a scan speed (2θ) of 2°/min, a step size of 0.02. Unit cell parameters were calculated with the least-square method.

2.2.6. Nitrogen adsorption-desorption analysis

Nitrogen adsorption-desorption isotherms were collected at 77 K using a Quantachrome (NOVA 2200e) analyzer and the NovaWin software to assess the surface area, pore size, and pore volume of HAp. Before the analysis, the sample was degassed at 200 °C for 3 hours. The surface area was calculated using the MultiPoint Brunauer-Emmett-Teller (BET) method and the size and pore volume using the Density Functional Theory (DFT) method.

2.2.7. Point of zero charge (pH_{pzc})

The pH_{pzc} was evaluated using 0.1 M NaCl solutions with initial pH values (pH_i) from 2 to 12 adjusted by adding either 0.1 M HCl or 0.1 M NaOH. Then, 10 mg of HAp were added to 10 mL of NaCl solution and kept at constant stirring at room temperature using a magnetic stir plate (IKA® C-MAG HS 4). After 24 hours, once the equilibrium was reached, the suspensions were centrifuged at 12,096 × *g* for 10 min at 25 °C (Beckman Coulter Avanti J-26S XPI). The final pH values (pH_f) were measured in the supernatant using a potentiometer (Thermo Scientific® Orion 4-Star) and the difference between pH_i and pH_f ($\Delta pH=pH_i-pH_f$) was plotted against pH_i. The pH_{pzc} of HAp was determined by the intersection point of the resulting curve where ΔpH=0.

2.3. Dye adsorption

The adsorption capacity of HAp was measured using methyl orange (MO) dye in aqueous solution as indicated in the batch technique. A solution of 600 mg/L MO was used as stock; whereas the experimental solution was diluted from the stock solution to reach 150 mg/L. The final pH of the solution was 6, 75 mg of HAp were put in contact with 5 mL of MO experimental solution. The suspension was mixed on an orbital shaker (VWR®, Mini shaker) at 400 rpm for 24 hours at room temperature.

At the end of the experiment, the supernatant was centrifuged at 16,000 × *g* for 2 min at 25 °C (HERMLE, Z 36 HK High-Speed Centrifuge). The MO concentration was determined by measuring the absorbance of the solutions at λ_{max} 462 nm using a UV/VIS spectrophotometer (PerkinElmer, Lambda 20). The dye removal efficiency was calculated using HAp as adsorbent following the concentrations before and after the adsorption process.

3. Results and discussion

3.1. Hydroxyapatite (HAp) yield

The calcination temperature to synthesize HAp from fish bones has been reported in the range of 600-1200 °C (Sunil & Jagannatham, 2016; Venkatesan & Kim, 2010; Zhu et al., 2017). A temperature of 900 °C was selected since this ensures that HAp produced lacks organic moieties and water (Venkatesan & Kim, 2010). The HAp yield was 51.6 ± 0.7%, consistent with previous reports (Nam et al., 2019). Besides, the cleaning treatment used in this study offers the advantage of obtaining mince through the skeletons deboning and use the mince to develop value-added products (Lizárraga-Mata et al., 2016).

The production costs of HAp and the generation of residues would not increase because no additional substances are used for the sample preparation in comparison with those methods using alkaline or enzymatic hydrolysis (Nam et al., 2019). The calcination of fish bones is a simple, efficient, and cost-low method that allows obtaining good HAp yields without using precursors or the production of aggressive residues (Da Cruz et al., 2020). On the other hand, fish bones are abundant raw material, available and practically free of cost. Therefore, the process of obtaining HAp used in this study could be a feasible alternative for its large-scale application.

3.2. Identification and characterization of HAp

3.2.1. Thermogravimetric (TGA) and differential thermogravimetric (dTG) analyses

Figure 1 shows the TGA and dTG thermograms of tilapia bone powders. The temperature range was from 20 °C to 850 °C. Four stages of weight loss were observed. The first weight decrease (4.5%) occurred at <200 °C and was attributed to the release of water adsorbed on bone surface.

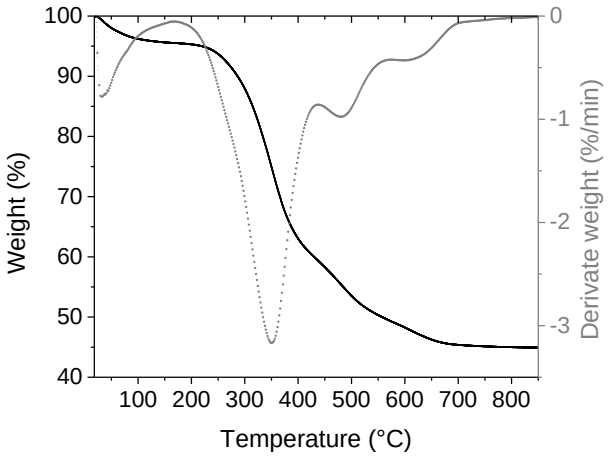

Figure 1. TGA (black continuous line) and dTG (gray dotted line) thermograms of tilapia bone powders.

The second stage was observed from 200-440 °C with a maximum peak at 350 °C. This stage has the most remarkable weight loss (36.5 %) and was related to crystal water removal from HAp and CO_2 and H_2O released from the partial combustion of organic matter such as proteins, collagen, and fat (Zhu et al., 2017). While at temperatures >440 °C, two weight losses (10% and 4%, respectively) took place, caused mainly by the carbonization process, beginning the dehydroxylation process from the apatite lattice (Ahmad Fara et al., 2015; Sofronia et al., 2014). Finally, at temperatures between 700 °C and 850 °C, there was only a 0.45% weight loss. At the end of the thermal process, the residual mass was 44.9 ± 5.2% attributed to inorganic matter in tilapia bones, *i.e.*, HAp.

3.2.2. Fourier transformed infrared spectroscopy (FTIR)

In Figure 2, the spectrum shows the characteristic peaks of HAp at 3571 cm^{-1} and 631 cm^{-1}, belonging to OH^- functional groups; while the peaks observed at 1093 cm^{-1}, 1047 cm^{-1}, 961 cm^{-1}, 603 cm^{-1}, 573 cm^{-1}, and 475 cm^{-1} are attributed to $(PO_4)^{3-}$. It is important to highlight that through both groups, OH^- and $(PO_4)^{3-}$, HAp can adsorb dye onto its surface (Adeogun et al., 2018). This is possible since these groups confer charge to HAp surface ($\equiv CaOH_2^+$, $\equiv CaO^-$ and $\equiv PO_4^-$), allowing the adsorption, mainly of cationic and anionic dyes, via electrostatic interactions (Bensalah et al., 2020; Wei et al., 2015). Furthermore, no functional groups related to organic compounds were observed, inferring that the heat treatment at 900 °C completely removed organic matter.

The HAp spectrum obtained in this work was like those previously reported for HAp obtained from Atlantic salmon (*Salmo salar*), sablefish (*Anoplopoma fimbria*), and sardine (*Sardinops melanostictus*) (Zhu et al., 2017).

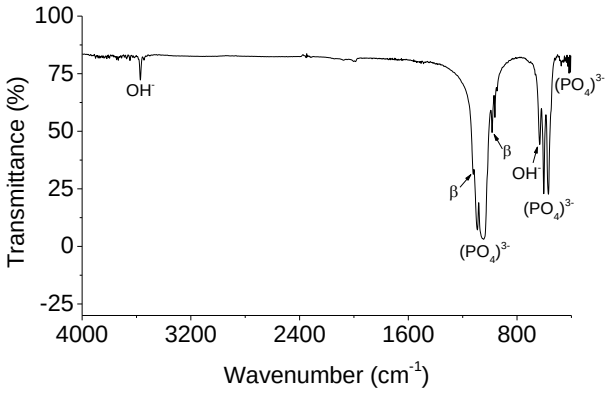

Figure 2. HAp instead Hap.

It has been reported that the formation of calcium phosphate is related to HAp that is not thermally stable (Venkatesan & Kim, 2010). In this sense, the spectrum of HAp (Figure 2) indicates the possible presence of β-tricalcium phosphate (β-TCP) with weak bands at 1122 cm^{-1} and 982 cm^{-1}, likely caused by the transformation of HAp to β-TCP phase at high calcination temperatures, beyond 650 °C (Paul, Pal, Choudhury, Bodhak, et al., 2017; Sunil & Jagannatham, 2016). In this sense, the presence of β-TCP was corroborated by the *XRD* methodology described in section *2.2.5.*

3.2.3. Field emission scanning electron microscopy (FESEM) and energy dispersive microscopy (EDS)

Figures 3a and 3c show HAp powders with different morphologies, including irregular, rod-like, and round shapes. They also show equiaxed grains of varied sizes forming agglomerates and aggregates with a submicron to micron size range. Moreover, a natural porous structure between particles became visible (Fig. 3a and c), probably due to the removal of organic substances, also appearing to be interconnected at least to the sample surface (Fig. 3b), coinciding with previous reports (Niakan et al., 2015; Zhu et al., 2017).

The energy dispersive microscopy (EDS) analysis (Figure 3d) revealed the presence of O, Ca, and P as main constituent elements, as well as small amounts of Mg, Na, S, and Al. It is common to find trace elements when HAp is obtained from natural sources, and these vary depending on nutrition and the turnover rate of the mineral (Niakan et al., 2015; Paul, Pal, Choudhury, Bodhak, et al., 2017). The XPS analysis confirmed a Ca/P molar ratio of 1.60, lower than the stoichiometric value of 1.67 for pure HAp. This result could be attributed to the formation of an additional phase in HAp as β-TCP with a Ca/P molar ratio of 1.50. It has also been reported that the content of trace elements in fishbone can affect the HAp Ca/P molar ratio (Goto & Sasaki, 2014). Increasing this ratio would be ad-

vantageous for the adsorption of acid dyes, the variation of Ca/P molar ratio could directly influence the adsorption efficiency of HAp, which depends on the acid-base nature of dyes (Bee & Hamid, 2020).

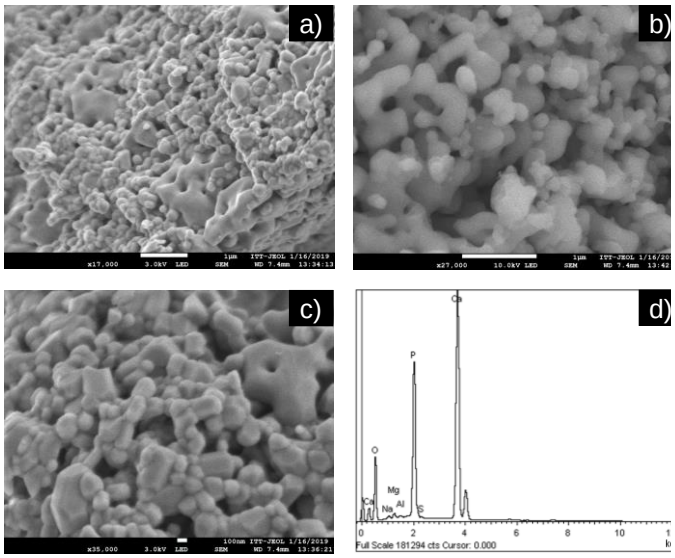

Figure 3. FESEM images of HAp powders at different magnifications a) 17000x, b) 27000x, c) 35000x and d) EDS spectrum.

3.2.4. Transmission electron microscopy (TEM)

HAp powders were characterized by TEM to observe their morphology clearly; likewise, the particle size was measured through TEM micrographs. Different shapes were observed, highlighting the rod-like shape (Fig. 4 a-c), in addition to the formation of agglomerates promoted by the fusion among particles (Fig. 4a). This could favor the presence of void pores in HAp powders (Fig. 4a and 4b); therefore, it could promote porosity, a desirable feature for adsorbent materials.

The particle size distribution of HAp was in the range of 100-2000 nm (Figure 4d). This broad distribution could be due to the coexistence of unfused and agglomerated particles. The average particle length was 655.1 ± 389.9 nm; this result agrees with the particle size range reported for HAp obtained from fish bones by calcination (Da Cruz et al., 2020; Sunil & Jagannatham, 2016; Zhu et al., 2017).

Particle size plays a significant role in the adsorption capacity of dyes, smaller particles show better adsorption capacity because of their specific area increment (Aljeboree et al., 2017). Therefore, more active sites are available for adsorption. Adsorption capacity could also be influenced by the ability of the dye to penetrate the internal pores of the particles. However, this ability is associated with the molecular size of the dye. In this sense, Aljeboree et al. (2017) revealed that the relationship between adsorption capacity and particle size depends on (i) the chemical structure of the dye molecule and (ii) the intrinsic characteristics of the adsorbent.

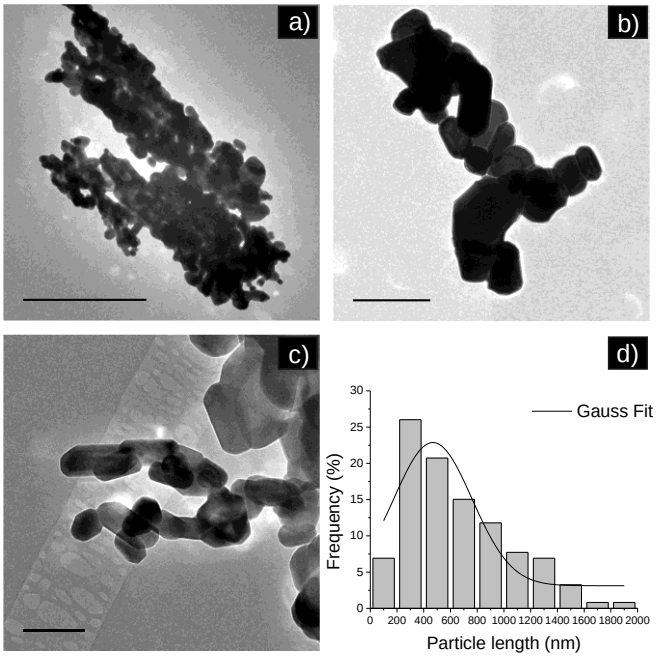

Figure. 4. TEM images a), b), c) of HAp powders and d) particle size distribution with Gaussian fit.

3.2.5. X-Ray Diffraction (XRD)

The XRD results for the sample showed that HAp was the predominant phase. Figure 5 shows the XRD pattern of the sample and the simulated HAp pattern (ICDD card No. 00-009-0432, hexagonal system, *a* (Å)= 9.4180, *c* (Å)= 6.8840, V (Å)= 528.80, space group P63/m, no. 176) for comparison. The unit cell parameters of the sample were 9.418 Å and 6.884 Å for the *a* and *c* parameters, respectively, and the volume was 528.78 $Å^3$. These results were like those previously reported for HAp obtained from fish bones such as sheelavati (*Roho labio*) and barramundi (*Lates calcarifer*) (Paul, Pal, Choudhury, Balla, et al., 2017; Sunil & Jagannatham, 2016).

Additional peaks corresponding to crystallographic planes of β-TCP phase from ICDD card. No. 00-009-0169 was observed. These results were consistent with those shown in section *3.2.2 FTIR*, where bands associated with β-TCP appeared, and with the findings of section *3.2.3 FESEM* and *EDS*, where the Ca/P ratio was 1.60, associated with the presence of β-TCP. According to Dastoorian et al. (2018), the formation of tricalcium phosphate phases may not affect the adsorption of dye on HAp.

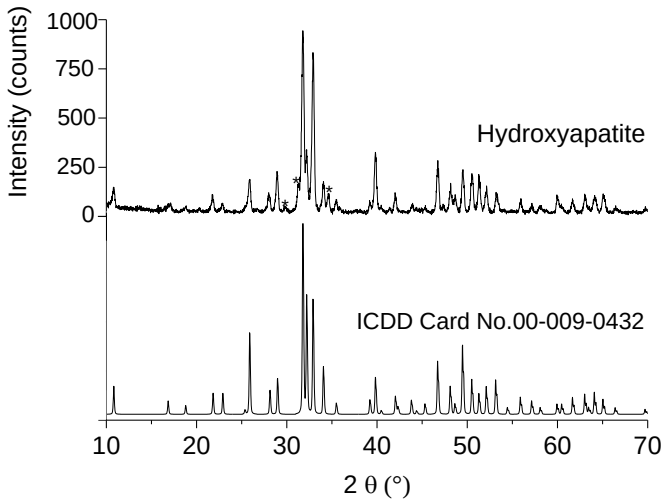

Figure. 5. XRD pattern of HAp obtained at 900 °C, ICDD card No. 00-009-0432 for pure HAp, and (*) peaks attributed to β-TCP.

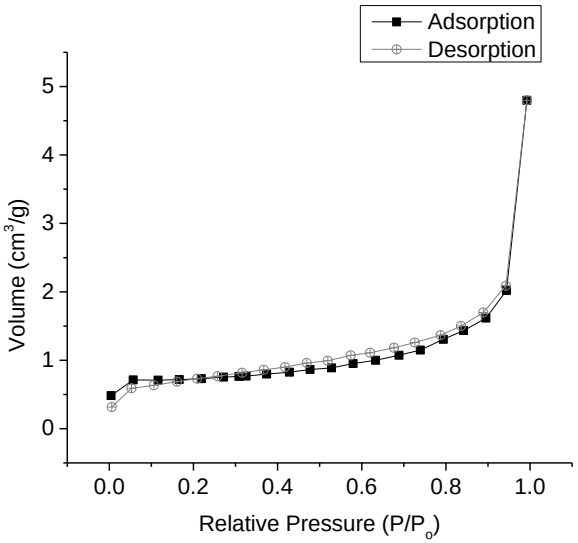

Figure 6. Nitrogen adsorption-desorption of HAp.

3.2.6. Nitrogen adsorption-desorption analysis

The nitrogen adsorption-desorption isotherm of HAp is shown in Figure 6, according to the IUPAC it corresponds to a type II isotherm, common for macroporous or non-porous adsorbents (Thommes et al., 2015). The surface area, pore-volume, and pore size (diameter) observed were 2.29 m^2/g, 0.003 cm^3/g, and 1.5 nm, respectively. Although the surface area corresponded with that reported for HAp obtained from fish bones by calcination process (1.65-32.38 m^2/g) (Nam et al., 2019); it was lower than those reported from activated carbons, one of the most used adsorbents due to their high adsorption capacity attributed to their high surface area and pore volume (Álvarez-Torrellas et al., 2017).

Therefore, based on the type of isotherm and the texture values of the HAp, this material could be considered non-porous. The high temperatures used in this kind of synthesis method could trigger fusion between the HAp particles. These agglomerates could produce low values of texture properties compared to those where high temperatures are not used (Guan et al., 2018).

It is well-known that the textural characteristics of adsorbents significantly affect adsorption, and that the surface chemistry could favor the adsorbent-adsorbate interaction (Scheufele et al., 2020). However, a previous study revealed a non-abundant porous structure (0.0776 cm^3/g) and a low surface area (15.076 m^2/g) for HAp, exhibiting a large adsorption amount of methylene blue, indicating that textural properties were independent of the dye removal capacity (Chen et al., 2020). Therefore, HAp obtained in this study could show a good adsorption of the dyes contained in the effluents discarded by the textile industry.

3.2.7. Point of zero charge (pH_{pzc})

The pH_{pzc} value obtained for HAp was 9.7 (Fig. 7), close to the values previously reported for HAp from shell powder (Nayak & Misra, 2019; Xia et al., 2019). At a pH lower than pH_{pzc} the HAp surface is positively charged, while at a pH higher than pH_{pzc} the surface charge becomes negative. Therefore, the adsorption of anionic and cationic dyes on HAp could be promoted at a pH< 9.7 and at a pH> 9.7, respectively. In both cases, electrostatic attraction could be the main adsorption mechanism involved (Chen et al., 2020; Guan et al., 2018).

Considering that the permissible limit of pH for the effluents from the textile industry should be from 6 to 9 (Li et al., 2017) and that at this range the HAp surface is positively charged, HAp obtained could be used to remove anionic dyes such as Congo red (CR), reactive black 5 (RB5), methyl orange (MO), among others. However, the pH levels of the effluents from the textile industry are commonly high or close to 12 (Islam & Guha, 2013), in this sense, cationic dyes could also be removed with HAp.

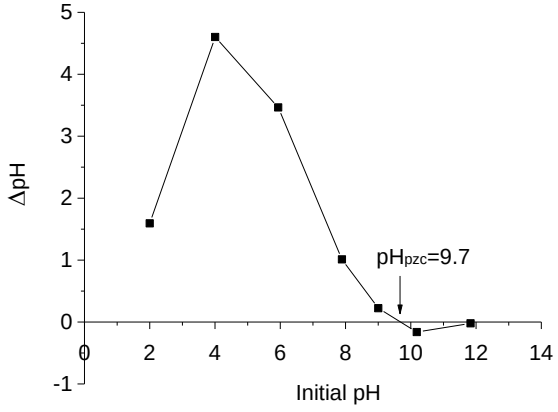

Figure 7. Point of zero charge (pH_{pzc}) of the HAp.

3.3. Dye adsorption using methyl orange (MO) as a model

Figures 8a and 8b show MO solution before and after the dye adsorption process. HAp was able to remove 82.6 ± 0.9% of MO from the aqueous solution, similar to a previous study where an anionic dye was adsorbed on HAp (Adeogun et al., 2018). Electrostatic interactions are the main mechanism proposed in the literature for dye adsorption on HAp (Chen et al., 2020; Guan et al., 2018). In this sense, it is suggested that MO dye adsorption onto HAp could occur through the electrostatic interactions between SO_3^- groups of MO dye and Ca^{2+} ions of HAp.

The pH 6 of the experimental solution of MO used in this study (pH < pH_{pzc}) could also have favored HAp surface to be positively charged, thereby promoting the anionic dye adsorption on HAp.

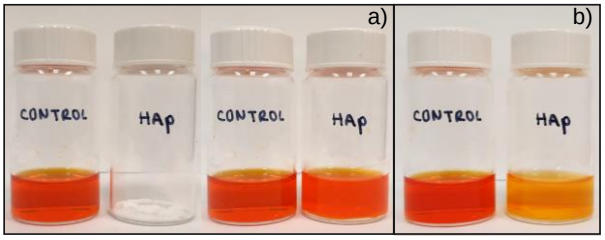

Figure. 8. MO solution a) before and b) after the adsorption on HAp.

4. Conclusions

Hydroxyapatite (HAp) from tilapia (*Oreochromis niloticus*) bones was successfully obtained by a calcination process. The characterization techniques revealed that the chemical composition, morphology, particle size, and texture are suitable properties suggesting the use of HAp as a convenient dye adsorbent. Methyl orange (MO) used as a model dye revealed the capacity of HAp for anionic dye adsorption from aqueous solution.

The findings of this work represent a meaningful approach towards the use of HAp from tilapia (*Oreochromis niloticus*) bones as a potential candidate for dye removal. Further studies will be carried in out our laboratory to evaluate the factors affecting the adsorption process such as dye initial concentration, adsorbent dose, pH and solution temperature, among others.

Conflict of interest

The authors do not have any type of conflict of interest to declare.

Acknowledgements

The Doctorate in Material Science for the student Beatriz Guadalupe González-González was supported by Consejo Nacional de Ciencia y Tecnología (CONACYT, Mexico) [Scholarship No. 697497]. We gratefully acknowledge the use of the facilities and the technical assistance of the TEM and XPS laboratories at the University of Sonora (Physical and Polymers Departments). We also express our gratitude to Dr. Fabricio Espejel-Ayala from the Center for Research and Technological Development in Electrochemistry (CIDETEQ) for his help in collecting XRD data.

Funding

The authors received no specific funding for this work.

References

Abdel-Ghany, H. M., El-Sayed, A.-F. M., Ezzat, A. A., Essa, M. A., & Helal, A. M. (2019). Dietary lipid sources affect cold tolerance of Nile tilapia (*Oreochromis niloticus*). *Journal of Thermal Biology*, *79*, 50–55. https://doi.org/10.1016/j.jtherbio.2018.11.009

Adeogun, A. I., Ofudje, E. A., Idowu, M. A., Kareem, S. O., Vahidhabanu, S., & Babu, B. R. (2018). Biowaste-Derived Hydroxyapatite for Effective Removal of Reactive Yellow 4 Dye: Equilibrium, Kinetic, and Thermodynamic Studies. *ACS Omega*, *3*(2), 1991–2000. https://doi.org/10.1021/acsomega.7b01768

Ahmad Fara, A. N. K., bin Yahya, M. A., & Abdullah, H. Z. (2015). Preparation and Characterization of Biological Hydroxyapatite (HAp) Obtained from Tilapia Fish Bone. *Advanced Materials Research*, *1087*, 152–156. https://doi.org/10.4028/www.scientific.net/AMR.1087.152

Akhouairi, S., Ouachtak, H., Addi, A. A., Jada, A., & Douch, J. (2019). Natural Sawdust as Adsorbent for the Eriochrome Black T Dye Removal from Aqueous Solution. *Water, Air, & Soil Pollution*, *230*(8), 181. https://doi.org/10.1007/s11270-019-4234-6

Aljeboree, A. M., Alshirifi, A. N., & Alkaim, A. F. (2017). Kinetics and equilibrium study for the adsorption of textile dyes on coconut shell activated carbon. *Arabian Journal of Chemistry*, *10*, S3381–S3393. https://doi.org/10.1016/j.arabjc.2014.01.020

Álvarez-Torrellas, S., Martin-Martinez, M., Gomes, H. T., Ovejero, G., & García, J. (2017). Enhancement of p-nitrophenol adsorption capacity through N_2-thermal-based treatment of activated carbons. *Applied Surface Science*, *414*, 424–434. https://doi.org/10.1016/j.apsusc.2017.04.054

Bee, S.-L., & Hamid, Z. A. A. (2020). Hydroxyapatite derived from food industry bio-wastes: Syntheses, properties and its potential multifunctional applications. *Ceramics International*, *46*(11), 17149–17175. https://doi.org/10.1016/j.ceramint.2020.04.103

Benkhaya, S., M' rabet, S., & El Harfi, A. (2020). A review on classifications, recent synthesis and applications of textile dyes. *Inorganic Chemistry Communications*, *115*, 107891. https://doi.org/10.1016/j.inoche.2020.107891

Bensalah, H., Younssi, S. A., Ouammou, M., Gurlo, A., & Bekheet, M. F. (2020). Azo dye adsorption on an industrial waste-transformed hydroxyapatite adsorbent: Kinetics, isotherms, mechanism and regeneration studies. *Journal of Environmental Chemical Engineering*, *8*(3), 103807. https://doi.org/10.1016/j.jece.2020.103807

Ceretta, M. B., Vieira, Y., Wolski, E. A., Foletto, E. L., & Silvestri, S. (2020). Biological degradation coupled to photocatalysis by ZnO/polypyrrole composite for the treatment of real textile wastewater. *Journal of Water Process Engineering*, *35*, 101230. https://doi.org/10.1016/j.jwpe.2020.101230

Chaari, I., Fakhfakh, E., Medhioub, M., & Jamoussi, F. (2019). Comparative study on adsorption of cationic and anionic dyes by smectite rich natural clays. *Journal of Molecular Structure*, *1179*, 672–677. https://doi.org/10.1016/j.molstruc.2018.11.039

Chen, X., Li, P., Zeng, X., Kang, Y., Wang, J., Xie, H., Liu, Y., & Zhang, Y. (2020). Efficient adsorption of methylene blue by xanthan gum derivative modified hydroxyapatite. *International Journal of Biological Macromolecules*, *151*, 1040–1048. https://doi.org/10.1016/j.ijbiomac.2019.10.145

Da Cruz, J. A., Weinand, W. R., Neto, A. M., Palácios, R. S., Sales, A. J. M., Prezas, P. R., Costa, M. M., & Graça, M. P. F. (2020). Low-Cost Hydroxyapatite Powders from Tilapia Fish. *JOM*, *72*(4), 1435–1442. https://doi.org/10.1007/s11837-019-03998-4

Darwish, A. A. A., Rashad, M., & AL-Aoh, H. A. (2019). Methyl orange adsorption comparison on nanoparticles: Isotherm, kinetics, and thermodynamic studies. *Dyes and Pigments*, *160*, 563–571. https://doi.org/10.1016/j.dyepig.2018.08.045

Dastoorian, F., Salem, A., & Salem, S. (2018). Fabrication of poorly crystalline hydroxyapatite nano-particles by rapid auto-ignition route as efficient adsorbent for removal of disperse blue dye. *Journal of Alloys and Compounds*, *766*, 729–738. https://doi.org/10.1016/j.jallcom.2018.07.042

Dotto, J., Fagundes-Klen, M. R., Veit, M. T., Palácio, S. M., & Bergamasco, R. (2019). Performance of different coagulants in the coagulation/flocculation process of textile wastewater. *Journal of Cleaner Production*, *208*, 656–665. https://doi.org/10.1016/j.jclepro.2018.10.112

El Haddad, M., Mamouni, R., Saffaj, N., & Lazar, S. (2012). Removal of a cationic dye–Basic Red 12–from aqueous solution by adsorption onto animal bone meal. *Journal of the Association of Arab Universities for Basic and Applied Sciences*, *12*(1), 48-54. https://doi.org/10.1016/j.jaubas.2012.04.003

FAO. (2020). *The State of World Fisheries and Aquaculture 2020*. FAO. https://doi.org/10.4060/ca9229en

Goto, T., & Sasaki, K. (2014). Effects of trace elements in fish bones on crystal characteristics of hydroxyapatite obtained by calcination. *Ceramics International*, *40*(7), 10777–10785. https://doi.org/10.1016/j.ceramint.2014.03.067

Guan, Y., Cao, W., Wang, X., Marchetti, A., & Tu, Y. (2018). Hydroxyapatite nano-rods for the fast removal of congo red dye from aqueous solution. *Materials Research Express*, *5*(6), 065053. https://doi.org/10.1088/2053-1591/aaccb8

Islam, A., & Guha, A. K. (2013). Removal of pH, TDS and color from textile effluent by using coagulants and aquatic/non aquatic plants as adsorbents. Resources and Environment, 3(5), 101–114.

Li, Y., Lu, L., Tan, Y., Wang, L., & Shen, M. (2017). Decoupling Water Consumption and Environmental Impact on Textile Industry by Using Water Footprint Method: A Case Study in China. *Water*, *9*(2), 124. https://doi.org/10.3390/w9020124

Lizárraga-Mata, W. L., García-Sifuentes, C. O., Scheuren-Acevedo, S. M., Lugo-Sánchez, M. E., Zamorano-García, L., Ramirez-Suárez, J. C., & Martinez-Porchas, M. (2016). Mince from Tilapia-Backbone: Effects of Washing and Cryoprotectant Addition during Frozen Storage. *Journal of Food Research*, *5*(5), 32. https://doi.org/10.5539/jfr.v5n5p32

Nam, P. V., Hoa, N. Van, & Trung, T. S. (2019). Properties of hydroxyapatites prepared from different fish bones: A comparative study. *Ceramics International*, *45*(16), 20141–20147. https://doi.org/10.1016/j.ceramint.2019.06.280

Nayak, B., & Misra, P. K. (2019). Recognition of the surface characteristics and electrical properties of a nanocrystalline hydroxyapatite synthesized from Pila globosa shells for versatile applications. *Materials Chemistry and Physics*, *230*, 187–196. https://doi.org/10.1016/j.matchemphys.2019.03.068

Niakan, A., Ramesh, S., Ganesan, P., Tan, C. Y., Purbolaksono, J., Chandran, H., Ramesh, S., & Teng, W. D. (2015). Sintering behaviour of natural porous hydroxyapatite derived from bovine bone. *Ceramics International*, *41*(2), 3024–3029. https://doi.org/10.1016/j.ceramint.2014.10.138

Paul, S., Pal, A., Choudhury, A. R., Balla, V. K., Das, M., & Sinha, A. (2017). Synthesis of hydroxyapatite from *Lates calcarifer* fish bone for biomedical applications. *Materials Letters*, *203*, 89–92. https://doi.org/10.1016/j.matlet.2017.05.103

Paul, S., Pal, A., Choudhury, A. R., Bodhak, S., Balla, V. K., Sinha, A., & Das, M. (2017). Effect of trace elements on the sintering effect of fish scale derived hydroxyapatite and its bioactivity. *Ceramics International*, *43*(17), 15678–15684. https://doi.org/10.1016/j.ceramint.2017.08.127

Peng, Q., Yu, F., Huang, B., & Huang, Y. (2017). Carbon-containing bone hydroxyapatite obtained from tuna fish bone with high adsorption performance for Congo red. *RSC Advances*, *7*(43), 26968–26973. https://doi.org/10.1039/C6RA27055G

Scheufele, F. B., Staudt, J., Ueda, M. H., Ribeiro, C., Steffen, V., Borba, C. E., Módenes, A. N., & Kroumov, A. D. (2020). Biosorption of direct black dye by cassava root husks: Kinetics, equilibrium, thermodynamics and mechanism assessment. *Journal of Environmental Chemical Engineering*, *8*(2), 103533. https://doi.org/10.1016/j.jece.2019.103533

Sofronia, A. M., Baies, R., Anghel, E. M., Marinescu, C. A., & Tanasescu, S. (2014). Thermal and structural characterization of synthetic and natural nanocrystalline hydroxyapatite. *Materials Science and Engineering C*, *43*, 153–163. https://doi.org/10.1016/j.msec.2014.07.023

Sunil, B. R., & Jagannatham, M. (2016). Producing hydroxyapatite from fish bones by heat treatment. *Materials Letters*, *185*, 411–414. https://doi.org/10.1016/j.matlet.2016.09.039

Swamiappan, S., Ganesan, S., Sekar, V., Devaraj, S., Subramanian, A., Ponnusamy, V. K., & Kathirvel, P. (2021). Effective removal of cationic methylene blue dye using nano-hydroxyapatite synthesized from fish scale bio-waste. *International Journal of Applied Ceramic Technology*, *18*(3), 902–912. https://doi.org/10.1111/ijac.13672

Thommes, M., Kaneko, K., Neimark, A. V., Olivier, J. P., Rodriguez-Reinoso, F., Rouquerol, J., & Sing, K. S. W. (2015). Physisorption of gases, with special reference to the evaluation of surface area and pore size distribution (IUPAC Technical Report). *Pure and Applied Chemistry*, *87*(9–10), 1051–1069. https://doi.org/10.1515/pac-2014-1117

Tony, M. A. (2020). Central composite design optimization of Bismarck Dye oxidation from textile effluent with Fenton's reagent. *Applied Water Science*, *10*(5), 108. https://doi.org/10.1007/s13201-020-01192-5

Uzunoğlu, D., & Özer, A. (2016). Adsorption of Acid Blue 121 dye on fish (*Dicentrarchus labrax*) scales, the extracted from fish scales and commercial hydroxyapatite: equilibrium, kinetic, thermodynamic, and characterization studies. *Desalination and Water Treatment*, *57*(30), 14109–14131. https://doi.org/10.1080/19443994.2015.1063091

Venkatesan, J., & Kim, S. K. (2010). Effect of Temperature on Isolation and Characterization of Hydroxyapatite from Tuna (*Thunnus obesus*) Bone. *Materials*, *3*(10), 4761–4772. https://doi.org/10.3390/ma3104761

Wei, W., Yang, L., Zhong, W. H., Li, S. Y., Cui, J., & Wei, Z. G. (2015). Fast removal of methylene blue from aqueous solution by adsorption onto poorly crystalline hydroxyapatite nanoparticles. Digest Journal of Nanomaterials and Biostructures, 10(4), 1343–1363.

Xia, X., Shen, J., Cao, F., Wang, C., Tang, M., Zhang, Q., & Wei, S. (2019). A facile synthesis of hydroxyapatite for effective removal strontium ion. *Journal of Hazardous Materials*, *368*, 326–335. https://doi.org/10.1016/j.jhazmat.2019.01.040

Zhu, Q., Ablikim, Z., Chen, T., Cai, Q., Xia, J., Jiang, D., & Wang, S. (2017). The preparation and characterization of HA/β-TCP biphasic ceramics from fish bones. *Ceramics International*, *43*(15), 12213–12220. https://doi.org/10.1016/j.ceramint.2017.06.082